PETER SIGMUND

CLASSICAL SCATTERING OF CHARGED PARTICLES BY MOLECULES

Single and Multiple Collisions at Small Angles

Det Kongelige Danske Videnskabernes Selskab
Matematisk-fysiske Meddelelser **39**, 11

Kommissionær: Munksgaard
København 1977

Table of Contents

Synopsis

The effect of *molecular geometry* on *single and multiple scattering of charged particles* off molecules is investigated theoretically. The treatment is based on *classical scattering* theory and is valid at small scattering angles. Two limiting cases are identified; a short-range limit where atoms within a molecule act as separate scattering centers, and a long-range limit, where a molecule acts as one scattering center. The transition region is shown to fall into the range of impact parameters corresponding to moderately screened Coulomb scattering, i.e., the typical *Thomas-Fermi scattering* region. General expressions are derived for single-collision cross sections valid in each limit and in the transition region, and for the half-widths of angular and lateral multiple-scattering distributions. Comments are made upon the behaviour of the shape of multiple-scattering profiles. Quantitative results are based on the *power approximation* to the Thomas-Fermi and Lenz-Jensen interaction. Comparison with recent experimental results on multiple-scattering half-widths for the $Pb^{+}-N_2$ system shows excellent agreement. Even more pronounced effects are predicted for polyatomic molecules.

Printed in Denmark by Bianco Lunos Bogtrykkeri A/S. ISBN 87-7304-080-0

1. Introduction

When asked to describe the interaction between an energetic particle and a molecule, you will most likely choose one of two simplifications as your starting point. Either you consider the molecule as one target particle, with a suitably simplified shape (spherical, linear, etc.), or you treat it as being composed of independent atoms. Which of the two simplifications you will judge to be the more appropriate one depends on the effective range of interaction. In typical molecular-beam experiments, at *eV* energies or below, collision partners interact at distances well up to, and greater than, internuclear distances in molecules, hence the first description is likely to be preferred. Conversely, *MeV* or more energetic particles have their most violent encounters at very small internuclear distances, whence the second description might seem more appropriate. Indeed, a very customary approach to penetration problems in molecular solid or gaseous targets is to ignore molecular structure altogether, and to consider instead a mixture of randomly distributed atoms of the right overall density and composition.

There must be an intermediate situation where neither description is appropriate. As an example, let the typical interaction distance be of the order of one half the internuclear distance in a binary target molecule, and let the target be a dilute gas of such binary molecules. Then, every collision of the projectile with one target atom is accompanied by another collision with the other atom in the molecule. While the impact parameter specifying the first collision is distributed at random, the corresponding quantity for the second collision is obviously correlated. Whereas in an atomic gas of equal composition all collisions would obey a random distribution of impact parameters, only half of them do so in the molecular gas. Thus, molecular geometry has an influence on the spectral distribution of energy loss, deflection angles, and excitation phenomena. It is the purpose of this paper to investigate the influence of molecular geometry on small-angle single and multiple scattering of a beam of charged particles penetrating a molecular gas. In a related paper, the corresponding problem of energy loss is treated[1]. A short note reporting some conclusions of the present work as well as experimental results on multiple scattering by molecules has appeared recently[2].

The geometric effects discussed in this paper are characteristic of such scattering processes where the trajectory of the scattered particle as well as the location of the scatterer are well-defined in terms of a classical-orbit picture. There is a broad range of heavy-particle scattering processes, initial energies, and scattering angles where the scattering cross sections derived from classical dynamics can be applied in the analysis. These include the scattering of *MeV* fission fragments in solids or gases at the one end, and the scattering of *keV* or even *eV* helium and hydrogen ions in dilute gas targets at the other end. Criteria for the validity of a classical-orbital picture have been established[3,4], and are fulfilled in those cases where numerical results are given in this paper. Experimental work has been reviewed recently[5,6].

The present analysis has been developed in close analogy and simultaneously with related work on energy loss[1], and the outline of this paper has been deliberately chosen to be that of a follow-up. Although the presentation is hopefully self-contained, you may find it advantageous to first have a look at the simpler, 1-dimensional problem of energy loss.

2. General Description

Let a charged particle (usually an energetic ion) pass by a molecule (Fig. 1) at a vector distance $\mathbf{p}$ from some point Q that specifies the position of the molecule. Throughout this paper, we only consider situations where the deflection of the projectile at the molecule (and at its constituent atoms) is so small that the trajectory can be approximated by a straight line over the range of interaction with the molecule. This implies high velocity and/or large impact parameter $p(= |\mathbf{p}|)$. Within the region of validity of classical scattering, the ion is scattered by some angle

$$\varphi = \varphi(\mathbf{p}, \Omega),$$

where Ω stands for three or two angles that specify the orientation of the target molecule with respect to the direction of motion of the projectile. We shall assume that φ is also small in an absolute sense, such that the direction of motion of a scattered ion is determined by a small increment

$$\boldsymbol{\varphi} = \boldsymbol{\varphi}(\mathbf{p}, \Omega) \tag{1}$$

to be added (and perpendicular to) the unit vector along the initial direction (Fig. 1). With that direction representing a polar axis, we can introduce an "impact plane" perpendicular to it; this plane contains the 2-dimensional

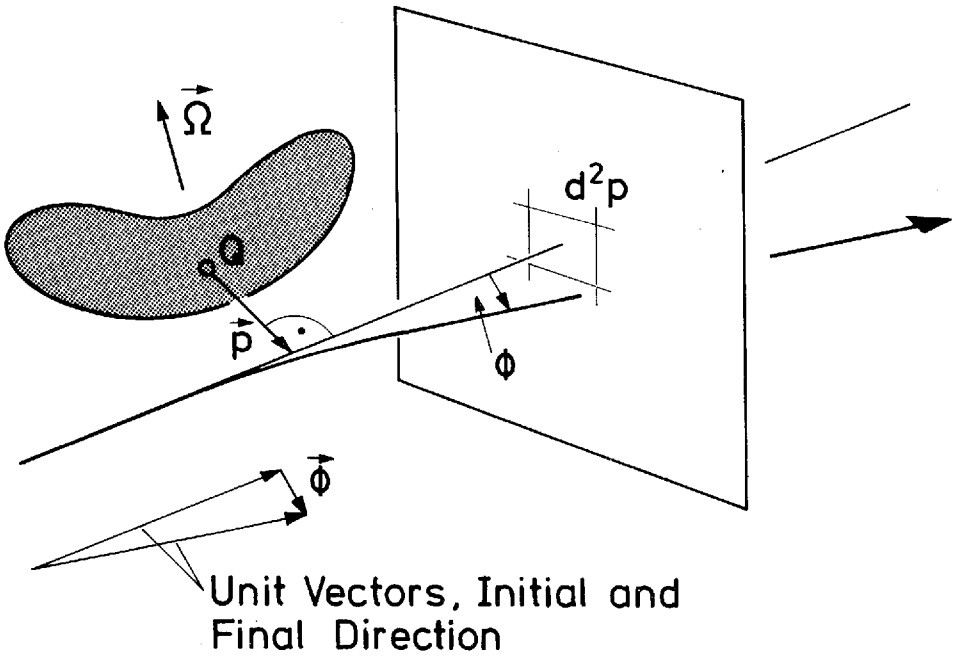

Fig. 1. Geometry of charged-particle scattering on a molecule.

vectors $\mathbf{p}$ and φ. In accordance with the conventional concept of a cross section we denote the quantity

$$d\sigma \equiv K(\varphi)d^2\varphi = d^2\varphi\int d^2\mathbf{p}\,\delta(\varphi - \varphi(\mathbf{p},\Omega)) \tag{2}$$

the differential cross section for scattering into the solid angle $d^2\varphi$ at φ, where δ is the Dirac delta funtion in two dimensions, and $d^2\mathbf{p}$ an element of the impact plane (Fig. 1).

Eq. (2) applies to a polarized gas, i.e. where all target molecules have the same orientation Ω. For random orientation, we generalize (2) so that

$$K(\varphi) = \int d^2\mathbf{p}\langle\delta(\varphi - \varphi(\mathbf{p},\Omega))\rangle_\Omega\,, \tag{2'}$$

where $\langle\ldots\rangle_\Omega$ indicates an average over all orientations.

It will be convenient in the following to carry on the analysis in the Fourier space conjugate to φ. In order to avoid the complications of a possible divergency at $\varphi = 0$, we consider the transport cross section

$$\sigma(\mathbf{k}) = \int d^2\varphi K(\varphi)(1 - e^{i\mathbf{k}\cdot\varphi}) = \int d^2\mathbf{p}\langle(1 - e^{i\mathbf{k}\cdot\varphi(\mathbf{p},\Omega)})\rangle_\Omega\,, \tag{3}$$

from which the differential cross section can be recovered[7] by inverse Fourier transformation,

$$K(\varphi) = -\frac{1}{(2\pi)^2}\int d^2k\ \sigma(\mathbf{k})e^{-i\mathbf{k}\cdot\varphi} \quad \text{for} \quad \varphi \neq 0. \tag{4}$$

3. Binary Molecules. General

Let us first consider a binary target molecule. The total deflection φ is then composed of two parts,

$$\varphi = \varphi_1 + \varphi_2, \tag{5}$$

i.e., the respective (vectorial) scattering angles belonging to the constituent atoms 1 and 2 of the molecule. Such a division is straight forward in case of a hypothetical molecule consisting of two nonoverlapping target atoms. In real molecules, the region of overlapping electron shells is occupied by valence electrons; these contribute to scattering only in a certain class of (very soft) collisions. In cases where this is important, scattering regions for atoms 1 and 2 may have to be defined. In case of a minor contribution of valence electrons to the scattering potential, the above picture of a molecule consisting of two unperturbed target atoms appears acceptable. This implies that the *individual* scattering vectors in (5) exhibit radial symmetry,

$$\varphi_i = \varphi_i(\mathbf{p}_i) = \varphi_i(p_i)\mathbf{p}_i/p_i, \quad i = 1, 2. \tag{6}$$

where $\mathbf{p}_1$ and $\mathbf{p}_2$ are distance vectors from the two target nuclei to the trajectory (Fig. 2), and $p_i = |\mathbf{p}_i|$ the individual impact parameters.

Eq. (3) can now be written in the form

$$\sigma(\mathbf{k}) = \langle\int d^2\mathbf{p}(1 - e^{i\mathbf{k}\cdot(\varphi_1(\mathbf{p}_1)+\varphi_2(\mathbf{p}_2))}\rangle_\Omega\,, \tag{7'}$$

which can be rearranged in the form

$$\sigma(\mathbf{k}) = \sigma_1(\mathbf{k}) + \sigma_2(\mathbf{k}) + \delta\sigma(\mathbf{k}). \tag{7}$$

Here,

$$\sigma_i(\mathbf{k}) = \langle\int d^2\mathbf{p}(1 - e^{i\mathbf{k}\cdot\varphi_i(\mathbf{p}_i)})\rangle_\Omega \equiv \int d\sigma_i(1 - e^{i\mathbf{k}\cdot\varphi}); \quad i = 1, 2, \tag{8}$$

with $d\sigma_i(\varphi)$ being the differential cross section of atom i; because of (6), the rotational average has no effect on eq. (8). The following interference term remains,

$$\delta\sigma(\mathbf{k}) = -\langle\int d^2p(1 - e^{i\mathbf{k}\cdot\varphi_1(\mathbf{p}_1)})(1 - e^{i\mathbf{k}\cdot\varphi_2(\mathbf{p}_2)})\rangle_\Omega\,; \tag{9}$$

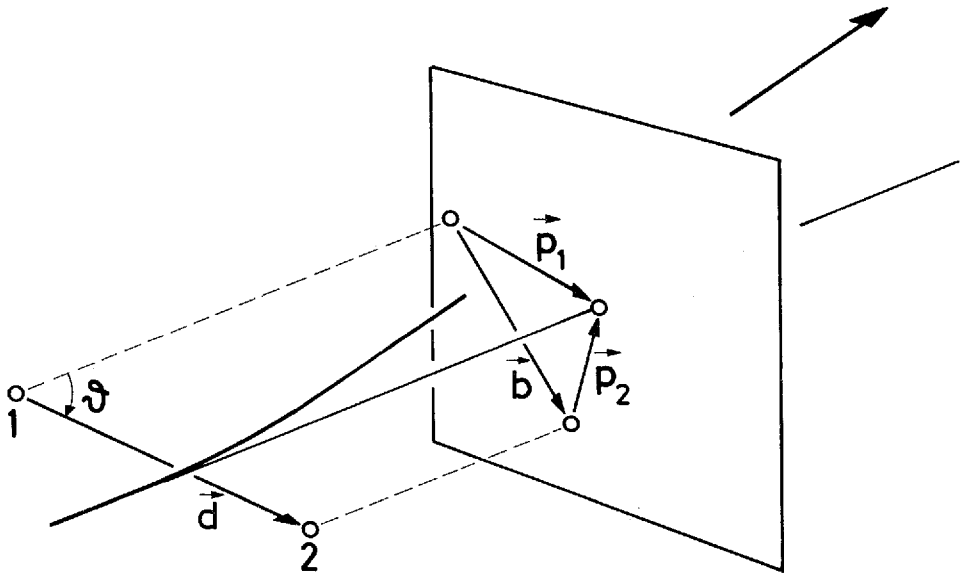

Fig. 2. Geometry of charged-particle scattering on a diatomic molecule.

this term is nonpositive, and composed of contributions from those impact parameters p_1 and p_2, and orientations Ω, where both φ_1 and φ_2 are nonzero. (The orientational dependence (Ω) is implicit in $\mathbf{p}_1$ and $\mathbf{p}_2$).

4. Binary Molecules. Evaluation of the Transport Cross Section

Let the internuclear distance vector in the molecule be $\mathbf{d}$, and its projection on the impact plane be $\mathbf{b}$. Then (Fig. 2),

$$\mathbf{b} = \mathbf{p}_1 - \mathbf{p}_2, \tag{10}$$

and

$$\delta\sigma(\mathbf{k}) = -\int d^2\mathbf{p}_1(1 - e^{i\mathbf{k}\cdot\varphi_1(\mathbf{p}_1)})\int d^2\mathbf{p}_2(1 - e^{i\mathbf{k}\cdot\varphi_2(\mathbf{p}_2)})\cdot\langle\delta(\mathbf{p}_1 - \mathbf{p}_2 - \mathbf{b})\rangle_\Omega. \tag{11}$$

The last factor in the integral has been evaluated previously[1]; it is easily found to be

$$\langle\delta(\mathbf{p}_1 - \mathbf{p}_2 - \mathbf{b})\rangle_\Omega = \frac{1}{2\pi d^2}(1 - (\mathbf{p}_1 - \mathbf{p}_2)^2/d^2)^{-1/2} \tag{12}$$

for $|\mathbf{p}_1 - \mathbf{p}_2| \leq d = |\mathbf{d}|$, and zero otherwise. In those situations where the integral (11) is made up mainly of contributions from impact parameters $|\mathbf{p}_1 - \mathbf{p}_2| \ll d$, we obtain from (11) and (12) the asymptotic relationship

$$\delta\sigma(\mathbf{k}) \sim -\frac{\sigma_1(\mathbf{k})\,\sigma_2(\mathbf{k})}{2\pi d^2}, \tag{13}$$

by means of eq. 8. Therefore, eq. 7 reads*

$$\sigma(k) = \sigma_1(k) + \sigma_2(k) - \frac{\sigma_1(k)\,\sigma_2(k)}{2\pi d^2} \ldots \text{ for "large } d\text{"} \tag{14}$$

In the opposite limit of a large interaction range ($\gg d$), Taylor expansion of the delta function in (11) yields

$$\langle \delta(\mathbf{p}_1 - \mathbf{p}_2 - \mathbf{b}) \rangle_\Omega = \delta(\mathbf{p}_1 - \mathbf{p}_2) + \frac{d^2}{6} \nabla^2_{\mathbf{p}_1} \delta(\mathbf{p}_1 - \mathbf{p}_2) \ldots$$

and, by direct evaluation of eq. (7'),

$$\sigma(\mathbf{k}) = \int d^2\mathbf{p} (1 - e^{i\mathbf{k}\cdot(\varphi_1+\varphi_2)}) - \frac{d^2}{6} \int d^2\mathbf{p} e^{i\mathbf{k}\cdot\varphi_2} \nabla^2_{\mathbf{p}} e^{i\mathbf{k}\cdot\varphi_1} \ldots \text{ for "small } d\text{"} \tag{15}$$

where φ_i now stands for $\varphi_i(\mathbf{p})$.

5. Power Scattering

The integrals that appeared in the previous section offer themselves for convenient evaluation in the particular case of power scattering

$$\varphi_i(p) = \frac{C_i}{p^s}; \qquad i = 1, 2 \tag{16}$$

with a positive parameter s. It is known[3–5] that within the small-angle approximation, (16) represents the scattering law for a repulsive interaction potential $\propto R^{-s}$ where R is the distance from the scattering center. The quantity C_i contains atomic parameters and is inversely proportional to the energy. Thus, at any given impact parameter p, the small-angle assumption can always be fulfilled by choice of a sufficiently high ion energy.

* *Note added in proof:* Eq. (14) is formally very similar to an expression derived by Glauber[18] for the forward scattering amplitude in GeV nucleon-deuteron scattering. The underlying physical effect in that case is a mutual shadowing of two independent scatterers. This shadowing effect has the same origin as the correlation effects considered in the present work as well as in previous work on energy loss[1], i.e., the geometric structure of the target particle, but it is otherwise different because of the rather different scattering mechanism. In particular, Glauber's treatment of diffraction scattering yields an interference term corresponding to (13) that is a factor of two smaller. I am grateful to N. Andersen for drawing my attention to a note referring to Glauber's work.

It is known that by proper choice of the power s, an accurate representation can be found for repulsive atomic interaction potentials[3], cross sections for screened-Coulomb scattering[4], and multiple-scattering profiles[8]. For the present purpose, the assumption of *one* exponent s applying to *both* atoms ($i = 1, 2$) is an important mathematical simplification. Except in case of very different masses of the constituent atoms, this assumption is not a severe physical limitation.

Inserting (16) into (8), we obtain[7]

$$\sigma_i(k) = A_i k^{2m} \tag{17}$$

with

$$A_i = \pi \frac{\Gamma(1-m)}{\Gamma(1+m)} (C_i/2)^{2m} \tag{17a}$$

and

$$m = 1/s \tag{17b}$$

Moreover, (15) reads

$$\sigma(k) = Ak^{2m} + Bd^2 + \ldots \tag{18}$$

with

$$A = (A_1^{s/2} + A_2^{s/2})^{2m} \tag{18a}$$

and

$$B = \frac{\pi}{3}(s-m) \frac{C_1 C_2}{(C_1 + C_2)^2}. \tag{18b}$$

6. Single Scattering. Differential and Incomplete Total Cross Section

After inserting (14) into (4), and observing (17) we obtain the following expression for the single-collision cross section of a diatomic molecule in the power approximation, in the limit of short-range interaction,

$$K(\varphi) = K_1(\varphi) + K_2(\varphi) - \frac{R(m)}{m} \cdot \frac{K_1(\varphi) K_2(\varphi) \varphi^2}{d^2} \ldots \tag{19'}$$

where

$$K_1(\varphi) = \frac{A_1 m}{\pi} \varphi^{-2-2m} \frac{2^{2m} \Gamma(1+m)}{\Gamma(1-m)} \tag{20}$$

and

$$R(m) = \frac{\Gamma(1+2m)\Gamma(1-m)^2}{\Gamma(1-2m)\,\Gamma(1+m)^2} \tag{21}$$

$R(m)$ has been plotted in fig. 3.

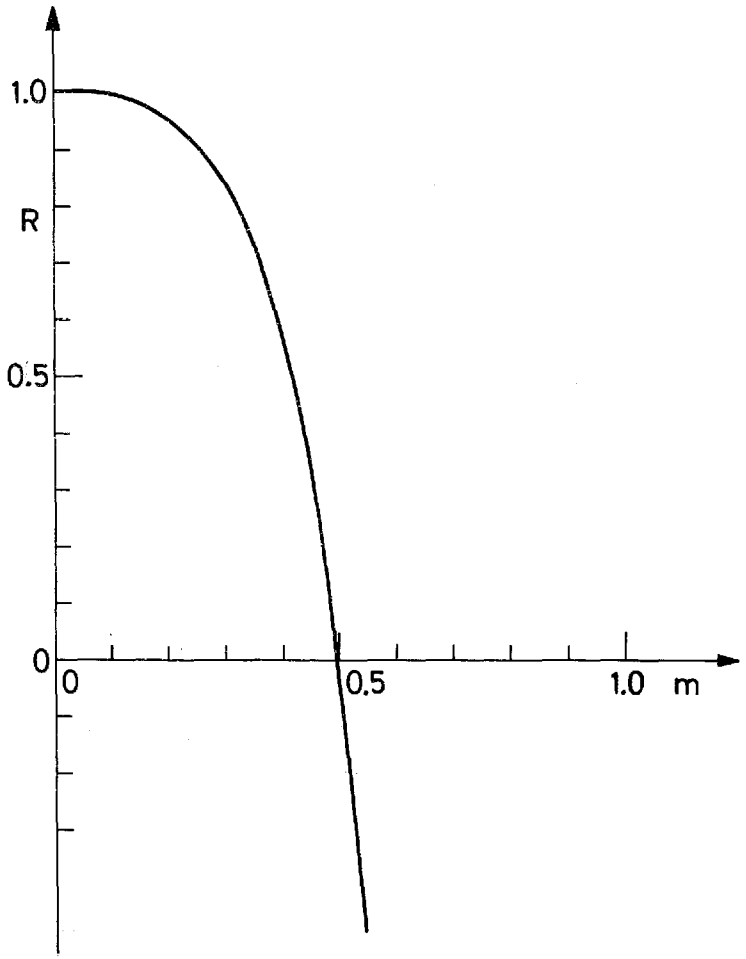

Fig. 3. The quantity R defined by (21), versus m.

In the (more familiar) notation

$$d\sigma \equiv K(\varphi)d^2\varphi \equiv \frac{d\sigma}{d\varphi}d\varphi, \tag{22}$$

(19') reads

$$\frac{d\sigma}{d\varphi} = \frac{d\sigma_1}{d\varphi} + \frac{d\sigma_2}{d\varphi} - \frac{R(m)}{m}\frac{\varphi}{2\pi d^2}\frac{d\sigma_1}{d\varphi}\frac{d\sigma_2}{d\varphi} + \ldots; \tag{19}$$

the subsequent term in the series would be proportional to d^{-4}. In the opposite limit of long-range interaction, eq. (18) yields

$$\left.\begin{aligned} K(\varphi) &= \frac{m}{\pi}\cdot A\cdot\varphi^{-2-2m}\frac{2^{2m}\Gamma(1+m)}{\Gamma(1-m)}+\ldots \\ &= [(K_1(\varphi))^{s/2}+(K_2(\varphi))^{s/2}]^{2m}+\ldots, \end{aligned}\right\} \quad (23)$$

and the subsequent term in the series would behave like $d^2\cdot\delta(\varphi)$; it has to be dropped, according to eq. (4).

In small-angle single-scattering experiments, it is most often the incomplete total cross section

$$\sigma_{\text{tot}} = \int_{\varphi_c}^{\pi} d\varphi \frac{d\sigma}{d\varphi} \quad (24)$$

which is the measured quantity. Here, φ_c is a (very small) limiting angle defined by the geometry of the apparatus. From eqs. (19) and (23) we obtain by integration

$$\sigma_{\text{tot}} = \sigma_{1,\text{tot}} + \sigma_{2,\text{tot}} - R(m)\frac{\sigma_{1,\text{tot}}\sigma_{2,\text{tot}}}{2\pi d^2}\ldots \quad (25)$$

for large d (short-range limit), and

$$\sigma_{\text{tot}} = [(\sigma_{1,\text{tot}})^{s/2}+(\sigma_{2,\text{tot}})^{s/2}]^{2m}+\ldots \quad (26)$$

for small d (long-range limit). Alternatively, (25) is a high-energy, and (26) a low-energy expansion.

Take, as an example, the case of a homonuclear binary molecule. Then, eqs. (19′), (19), and (25) represent the limit of a molecule consisting of two independent, identical scattering centers, and the apparent cross section is twice the cross section of a single atom (for $d\to\infty$). Conversely, eqs. (23) and (26) represent the case of a molecule acting as one target particle, the apparent cross section (averaged over all orientations) being 2^{2m} times the cross section of a single atom. This value is smaller (larger) than the former one provided that m is smaller (larger) than 1/2. The behaviour of the numerical factor $R(m)$ in (19′), (19), and (25) is consistent herewith: $R(m)\gtrless 0$ for $m\lessgtr 1/2$. Therefore, so long as the inter-atomic potential itself is reasonably close to a power potential, we can expect that the two limiting expansions, with some possible interpolation, describe the small-angle single-scattering cross section of a molecule satisfactorily. As will be shown in the following section, the short range limit (19) is appropriate in existing differential measurements, while it is not normally reached in measurements of the incomplete total cross section.

7. Application: Thomas-Fermi Scattering for Homonuclear Diatomic Target Molecule

Lindhard et al.[4] have given a very compact description of the elastic scattering between heavy atomic particles on the basis of a Thomas-Fermi (TF) interatomic potential. Their description hinges on the power-like behaviour of the TF potential over a moderately wide range of interaction energies. In their description[4],

$$d\sigma = \pi a^2 \frac{d\eta}{\eta^2} f(\eta) \tag{27}$$

where a is the screening radius of the interaction, and*

$$\eta = \varepsilon \sin \theta/2 \tag{28}$$

with θ the center-of-mass scattering angle, and ε the center-of-mass energy in units of $Z_1 Z_2 e^2/a$, Z_1 and Z_2 being atomic numbers of ion and target *atom*. $f(\eta)$ is some (given) universal function that can be approximated as

$$f(\eta) = \lambda \eta^{1-2m} \tag{29}$$

over limited regions of η, with λ a dimensionless constant depending on m, and m ranging from slightly greater than 0 to 1. $m = 1$ refers to Rutherford scattering.

In the small angle approximation, (28′) can be written in the form

$$\eta = \frac{E}{Z_1 Z_2 e^2/a} \cdot \frac{\varphi}{2} \equiv \tilde{\varphi}, \tag{28′}$$

where E is the laboratory energy, and the last part defines the scaled laboratory scattering angle $\tilde{\varphi}$. (21) reads, then

$$\frac{d\sigma}{d\tilde{\varphi}} = \frac{\pi a^2}{\tilde{\varphi}^2} f(\tilde{\varphi}) \quad \text{for} \quad \varphi \ll 1. \tag{27′}$$

The TF description is valid mostly at comparatively small interaction distances ($\lesssim a_0 = 0.529\,\text{Å}$). Therefore, the TF cross section for a diatomic homonuclear molecule is to be found primarily from eq. (19) which reads, by means of (27′)

* The notation $t^{1/2}$ is frequently found in the literature for η.

$$\left.\begin{aligned}\frac{d\sigma}{d\tilde{\varphi}} &= 2\frac{d\sigma_1}{d\tilde{\varphi}} - \frac{R(m)}{m}\frac{\tilde{\varphi}}{2\pi d^2}\left(\frac{d\sigma_1}{d\tilde{\varphi}}\right)^2 \cdots \\ &= \frac{2\pi a^2}{\tilde{\varphi}^2} f(\tilde{\varphi})\left[1 - \frac{R(m)}{4m}\cdot\frac{a^2}{d^2}\frac{f(\tilde{\varphi})}{\tilde{\varphi}} \cdots\right].\end{aligned}\right\} \quad (29')$$

In the limit of large E, i.e. large $\tilde{\varphi}$, the expression in brackets is small, and the molecule acts like two independent atoms. The case of strict Rutherford scattering ($m = 1$) has to be excluded, however, since the expansion (19) is not applicable in that case ($R(m = 1) = -\infty$). Pronounced deviations from the independent-atom picture occur at small values of $\tilde{\varphi}$, i.e. at low energies and/or small angles. In that case, ($\tilde{\varphi} \lesssim 0.1$) the TF interaction is described well by (29) with[9]

$$m = 1/3; \quad \lambda = 1.309, \tag{30}$$

and the factor in the brackets of (29) reads, then,

$$1 - 0.761\,\frac{a^2}{d^2}\tilde{\varphi}^{-2/3} \qquad \text{(TF)} \tag{31}$$

since $R(1/3) = 0.775$. For medium-mass collision partners we have[3, 4] $a \cong 0.885\, a_0(Z_1^{2/3} + Z_2^{2/3})^{-1/2} \sim 10^{-1}$ Å, i.e. $a^2/d^2 \sim 10^{-2}$. Hence, measurable deviations from 1 occur for $\tilde{\varphi} \lesssim 0.1$, and the expansion breaks down above $\tilde{\varphi} \sim 10^{-3}$. In fact, the low-energy limit (23) yields

$$d\sigma/d\tilde{\varphi} \to 2^{2/3}\, d\sigma_1/d\tilde{\varphi}; \tag{32}$$

this value is reached, according to (31), at

$$\tilde{\varphi} \approx 7\,\frac{a^3}{d^3},$$

i.e. around $\tilde{\varphi} \sim 10^{-2}$. Thus, the following qualitative picture arises for the small-angle scattering on molecular targets.

i) At scattering angles corresponding to $\tilde{\varphi} = \eta > 1$, a molecule behaves with high accuracy (better than 1 pct.) like two independent atoms.
ii) In the region $10^{-2} \lesssim \tilde{\varphi} \lesssim 1$ the cross section of a molecule becomes measurably smaller than that of two independent atoms.
iii) In the region $\tilde{\varphi} \lesssim 10^{-2}$ the cross section approaches the long-range limit.

Now, conventional small-angle scattering experiments that have been performed on molecular gas targets[5, 10] (in the σ_{tot}-geometry) dealt with impact parameters in the Born-Mayer region, where $\tilde{\varphi} < 10^{-3}$, and thus refer to the long-range limit. The analysis of those experiments has been based on a molecular picture. The present analysis confirms this picture but adds little new to it. In fact, it is oversimplified in this respect since valence electrons are important there, but are not taken into account explicitly.

Conversely, differential cross section measurements tend to deal with large enough angles and/or energies so that $\tilde{\varphi} > 1$, and the short-range limit should apply. A notable exception is Loftager's setup[11] where differential cross sections have been determined in the genuine TF region ($10^{-3} \lesssim \tilde{\varphi} < 10$), i.e. including the transition region between the long- and short-range limit. So far, mainly experiments with noble-gas targets have been performed, but pronounced molecular effects would be expected. Since, in that work, the atomic interaction appeared to be closer to a Lenz-Jensen (LJ) potential as characterized by (29) with[12]

$$m = 0.191; \qquad \lambda = 2.92 \tag{33}$$

at small values of η, we also quote the expression corresponding to (31) for LJ interaction,

$$1 - 3.68 \frac{a^2}{d^2} \tilde{\varphi}^{-0.382}; \tag{34}$$

the long-range limit $d\sigma/d\tilde{\varphi} \to 2^{0.382}\, d\sigma_1/d\tilde{\varphi}$ is reached around $\tilde{\varphi} = 500\,(a/d)^5 \sim 1/2 \cdot 10^{-2}$, i.e. at a similar value as in the TF case*.

8. Multiple Scattering. Angular and Lateral Distributions

In typical multiple-scattering experiments, either an angular distribution $F(x,\alpha)d\Omega$ of an initially collimated beam, or a lateral distribution $G(x,\varrho)d^2\rho$ is observed (fig. 4), where x is the travelled distance in the target. In the small-angle approximation, the angular distribution is given by Bothe's formula[7]

$$F(x,\alpha) = \frac{1}{2\pi} \int_0^\infty dk\, k\, J_0(k\alpha) e^{-N' x \sigma(k)}, \tag{35}$$

* Since the Lenz-Jensen interaction potential, contrary to the TF potential, does not approach power form at large inter-atomic distances, eqs. (29) and (33) approximate the LJ scattering law less accurately than eqs. (29) and (30) approximate the TF scattering law. In an accurate analysis of molecular scattering measurements, it may thus be necessary to explicitly include a dependence $m = m(\tilde{\varphi})$ in $R = R(m)$.

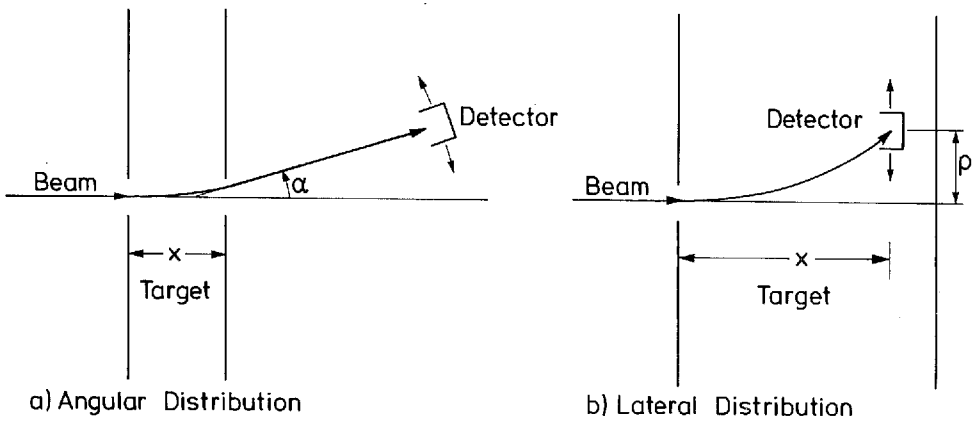

Fig. 4. Geometry of typical multiple-scattering experiments with gas targets.

where N' is the density of scattering centers and $\sigma(k)$ the transport cross section (3). Similarly[8],

$$G(x,\varrho) = \frac{1}{2\pi}\int_0^\infty \varkappa d\varkappa\, J_0(\varkappa\varrho)\exp\left(-N'\int_0^x dx'\sigma(\varkappa x')\right). \tag{39}$$

The two distributions are formally very similar and contain equivalent information. In addition, somewhat surprisingly, the two distributions scale very accurately even rather far out into the tails, as has been shown both theoretically[8] and experimentally[13]. It was found recently[8] that the power approximation for the transport cross section, as exemplified by eq. (17), serves as a very accurate basis for multiple-scattering theory in the screened-Coulomb region; it seems, in fact, more accurate than the actual underlying power potential and single-scattering cross section. The following considerations, therefore, have been based on the power approximation (17).

Let us apply eqs. (35) and (36) to *atomic* systems first. From (17) and (35), we find that k scales like $(N'x)^{-\frac{1}{2m}}/C_i$ and α like k^{-1}, i.e. $(N'x)^{\frac{1}{2m}}C_i$. In particular, the half-width $\alpha_{1/2}$ of $F(x,\alpha)$ must behave like

$$\alpha_{1/2} \propto (N'x)^{\frac{1}{2m}}/E, \tag{37}$$

since $C_i \propto 1/E$.

Similarly, from (17) and (36),

$$\varrho_{1/2} \propto (N'x)^{\frac{1}{2m}}\cdot\frac{x}{E}. \tag{38}$$

These variations have been checked experimentally in considerable detail. With regard to the present analysis, experiments with gases have been most convincing[13–15].

Let us, now, consider a diatomic gas, and let us assume, as in sect. 5, that one and the same power m governs collisions with both types of constituent atoms.

In the following, our reference standard is the completely dissociated gas of $N' = N/2$ atoms of type 1 and 2; N is the density of *atoms*. In that state, the exponent in the exponential function in (35) reads

$$-\frac{N}{2}x(\sigma_1 + \sigma_2) = -\frac{N}{2}x(A_1 + A_2)k^{2m} \tag{39}$$

A_1 and A_2 being defined in (17a).

In the long-range limit, (18a) yields instead,

$$-\frac{N}{2}x(A_1^{\frac{1}{2m}} + A_2^{\frac{1}{2m}})^{2m}k^{2m};$$

The latter expression takes on the form (39) if an apparent target thickness

$$x' = \frac{(C_1 + C_2)^{2m}}{C_1^{2m} + C_2^{2m}}x \tag{40a}$$

is introduced. Eq. (37) provides then the following relationship for the angular half-widths,

$$\frac{(\alpha_{1/2})_{\text{mol}}}{(\alpha_{1/2})_{\text{dissoc}}} = \left(\frac{x'}{x}\right)^{\frac{1}{2m}} \to \frac{C_1 + C_2}{(C_1^{2m} + C_2^{2m})^{\frac{1}{2m}}} \tag{41}$$

in the long-range limit. In particular, for homonuclear atoms, $C_1 = C_2$, (41) yields $2^{1-1/2m}$.

The same argument applied to (36) yields another apparent thickness

$$\left(\frac{x''}{x}\right)^{2m+1} = \frac{(C_1 + C_2)^{2m}}{C_1^{2m} + C_2^{2m}}. \tag{40b}$$

This, together with (38), provides a relationship between the lateral half-widths

$$\frac{(\varrho_{1/2})_{\text{mol}}}{(\varrho_{1/2})_{\text{dissoc}}} = \left(\frac{x'}{x}\right)^{1+\frac{1}{2m}} = \left(\left(\frac{x'}{x}\right)^{1+2m}\right)^{\frac{1}{2m}} = \frac{C_1 + C_2}{(C_1^{2m} + C_2^{2m})^{1/2m}} \tag{42}$$

i.e. exactly the same ratio as (41) in the short-range limit. In particular, this ratio becomes $2^{1-\frac{1}{2m}}$ for a homonuclear molecule. The angular and lateral half-widths $(\alpha_{1/2})_{\text{dissoc}}$ and $(\varrho_{1/2})_{\text{dissoc}}$ are comparable to atomic quantities that are known experimentally for a wide selection of ions and targets. The present argument makes use only of the scaling properties of the power cross section, i.e. of the experimental fact that the relations (37) and (38) are satisfied. The parameter m occurring in (41) and (42), in particular in the homonuclear case, is thus to be understood as the one extracted from measurements on the corresponding *atomic* systems.

The transition between the short- and long-range limit is harder to find. The argument has been outlined briefly in ref. 2. We note first that straight insertion of (14) into (35) or (36) with $\sigma_i(k)$ according to (17), would yield a spurious divergence at $k = \infty$, since the correction term $\delta\sigma(k)$ would be applied outside the region where it is small. Instead, a perturbation approach is taken.

Let us, first, insert (14) and (17) into (35). The exponent of the exponential function can be written in the form

$$\left.\begin{aligned} &- N'x(A_1 + A_2)k^{2m}\left[1 - \frac{A_1A_2}{A_1 + A_2} \cdot k^{2m}/2\pi d^2\right] \\ \approx\ &- N'x(A_1 + A_2)k^{2m}\left[1 - \frac{A_1A_2}{A_1 + A_2} \cdot k_0^{2m}/2\pi d^2\right] \end{aligned}\right\} \tag{43}$$

where k_0 is some representative value of k that will be specified below. This approximation is appropriate so long as the term in the brackets does not differ substantially from 1. It is also vital that k^{2m} varies slowly. (In the subsequent example, $m \approx 0.2$). Eq. (43) reduces the molecular correction to the independent-atom limit to an apparent target thickness x_1',

$$x_1' \simeq x\left(1 - \frac{A_1A_2}{A_1 + A_2}\frac{k_0^{2m}}{2\pi d^2}\right),$$

and thus, by means of (37)

$$\frac{(\alpha_{1/2})_{\text{mol}}}{(\alpha_{1/2})_{\text{dissoc}}} = \left(\frac{x_1'}{x}\right)^{\frac{1}{2m}} \simeq 1 - \frac{1}{2m}\frac{A_1A_2}{A_1 + A_2}\frac{k_0^{2m}}{2\pi d^2}. \tag{44}$$

Similarly, the exponent in (36) reads

$$\approx -N'(A_1+A_2)\varkappa^{2m}\frac{x^{2m+1}}{2m+1}\left\{1-\frac{2m+1}{4m+1}\frac{A_1A_2}{A_1+A_2}\frac{\varkappa_0^{2m}x^{2m}}{2\pi d^2}\right\} \tag{45}$$

with $\varkappa_0$ same representative value of $\varkappa$. Again, the molecular correction can be described by an apparent thickness x_1'' with

$$(x_1'')^{2m+1} = x^{2m+1}\left(1-\frac{2m+1}{4m+1}\frac{A_1A_2}{A_1+A_2}\frac{\varkappa_0^{2m}x^{2m}}{2\pi d^2}\right),$$

from which the lateral half-width can be found by means of (38)

$$\frac{(\varrho_{1/2})_{\mathrm{mol}}}{(\varrho_{1/2})_{\mathrm{dissoc}}} = \left(\frac{x_1''}{x}\right)^{1+\frac{1}{2m}} \cong 1-\frac{1}{2m}\frac{2m+1}{4m+1}\frac{A_1A_2}{A_1+A_2}\frac{\varkappa_0^{2m}x^{2m}}{2\pi d^2}. \tag{46}$$

The values of k_0 and $\varkappa_0$ need to be determined from the *unperturbed* integrals, i.e. the multiple-scattering distributions for the dissociated gas. According to (43), k_0^{2m} must scale like $[N'x(A_1+A_2)]^{-1}$; correspondingly (45) requires $\varkappa_0^{2m}$ to scale like $(2m+1)/[N'(A_1+A_2)x^{2m+1}]$. Therefore, (44) and (46) read

$$\frac{(\alpha_{1/2})_{\mathrm{mol}}}{(\alpha_{1/2})_{\mathrm{dissoc}}} \cong 1-\mathrm{const}\frac{1}{2m}\frac{1}{2\pi d^2N'x}\frac{A_1A_2}{(A_1+A_2)^2} \tag{44'}$$

$$\frac{(\varrho_{1/2})_{\mathrm{mol}}}{(\varrho_{1/2})_{\mathrm{dissoc}}} \cong 1-\mathrm{const}'\frac{1}{2m}\frac{(2m+1)^2}{4m+1}\frac{1}{2\pi d^2N'x}\frac{A_1A_2}{(A_1+A_2)^2} \tag{46'}$$

The values of the dimensionless constants in (44') and (46') depend on the precise definition of k_0 and $\varkappa_0$. Since the integrands in (35) and (36) are normally far from narrow, symmetric distributions, a choice based on extrema or zeros appears inappropriate. Instead, the median values have been chosen; moreover, for simplicity, we take median values at $\alpha = 0$, and $\varrho = 0$, respectively. The latter choice is justified because of the qualitative similarity of the contributions to the profile at any angle (or lateral spread) within the half-width.

It is easily shown (and specified in appendix A) that this choice yields

$$\mathrm{const} = \mathrm{const}' = g(m) \tag{47}$$

where g is the solution of the equation

$$\int_0^g dt\, t^{\frac{1}{m}-1}e^{-t} = \tfrac{1}{2}\int_0^\infty dt\, t^{\frac{1}{m}-1}e^{-t}. \tag{47a}$$

TABLE I. The quantity g as defined by eq. (47a), versus m.

m	g	m	g	m	g
1.000	0.694	0.250	3.671	0.143	6.671
0.667	1.184	0.222	4.170	0.133	7.171
0.500	1.678	0.200	4.672	0.125	7.669
0.400	2.175	0.182	5.170	0.118	8.171
0.333	2.675	0.167	5.673	0.111	8.669
0.286	3.174	0.154	6.170	0.105	9.167

The function $g(m)$ has been tabulated in table I.

The present discussion referred to the half-width of multiple scattering distributions rather than the full profile. The perturbation approach used precluded the consideration of a possible influence on the *shape* of the distributions by the molecular structure. A qualitative argument suggests that there is indeed such an influence. Take, as an example, the angular distribution $F(x,\alpha)$, and consider first the range of angles up to the half-width $\alpha_{1/2}$. The integral (35) receives, then, essential contributions from a certain range of k-values around the median value k_0. Now, with α increasing, the important range of k shifts towards smaller values because of the Bessel function, $J_0(k\alpha)$; consequently, the molecular correction becomes less important (cf. eq. (43)). Thus, at sufficiently large values of α the multiple-scattering profile for a molecular gas will approach the independent-atom solution, even though the half-width may be close to or within the long-range limit. This result is consistent with what has been found in the single-collision case, e.g., eq. (29′). A more quantitative consideration is sketched in appendix B.

9. Application: Multiple Scattering on Diatomic Homonuclear Molecules

Just as in sect. 7, the description can be simplified substantially in case of homonuclear molecules by the introduction of TF variables. These are well established in multiple-scattering theory (cf., e.g., refs. 7 and 8). We have

$$\tau = \pi a^2 N x \tag{48a}$$

$$\tilde{\alpha} = \frac{Ea}{2Z_1 Z_2 e^2}\alpha \tag{48b}$$

$$\tilde{\varrho} = \pi a^2 N \cdot \frac{Ea}{2Z_1 Z_2 e^2}\varrho \tag{48c}$$

where a is the Thomas-Fermi radius and $N = 2N'$ the number of atoms per unit volume. The latter choice has been made because it fits best to the dissociated gas as a reference standard. Inserting these definitions into (44′) and (46′), and regarding that $A_1 = A_2$ for homonuclear molecules, we finally obtain

$$\frac{(\tilde{\alpha}_{1/2})_{\mathrm{mol}}}{(\tilde{\alpha}_{1/2})_{\mathrm{dissoc}}} = \begin{cases} 1 - \dfrac{1}{2m}\left(\dfrac{a}{2d}\right)^2 \cdot \dfrac{g}{\tau} & \text{large } \tau \\ \text{for} & \\ 2^{1-\frac{1}{2m}} & \text{small } \tau \end{cases} \tag{49}$$

and

$$\frac{(\tilde{\varrho}_{1/2})_{\mathrm{mol}}}{(\tilde{\varrho}_{1/2})_{\mathrm{dissoc}}} = \begin{cases} 1 - \dfrac{1}{2m}\,\dfrac{(2m+1)^2}{4m+1}\left(\dfrac{a}{2d}\right)^2 \cdot \dfrac{g}{\tau} & \text{large } \tau \\ \text{for} & \\ 2^{1-\frac{1}{2m}} & \text{small } \tau \end{cases} \tag{50}$$

The upper relationships in (49) and (50) refer to the independent-atom or short-range limit. The lower values refer to the long-range limit. It is obvious that the relevant variable is the thickness parameter τ that also controls the half-widths[7, 8] $\tilde{\alpha}_{1/2}$ and $\tilde{\varrho}_{1/2}$: At large τ (large half-width) the short-range limit is appropriate, and the reverse is true at small τ.

The upper parts of eqs. (49) and (50) were already mentioned in a short note[2], where the notation

$$h(m) = \frac{2m+1}{4m+1}\, g(m) \tag{51}$$

was employed. Moreover, as was shown in ref. 8, the parameter m, which determines the interatomic potential, can be related in a definite way to the thickness parameter τ, eq. (48a), such that a function $m = m(\tau)$ can be defined for a given screened-Coulomb interaction potential. By means of these relationships for TF and Lenz-Jensen (LJ) interaction, one can relate g and h to τ directly (Fig. 5).

Fig. 6 shows experimental results of lateral half-widths measured with lead ions scattered on nitrogen and neon at the same density of atoms[2]. The TF screening radii are determined essentially by the heavy lead ions, so that from the point of view of comparison, neon ions should be an accurate substitute for nitrogen. The two full-drawn theoretical curves refer to eq. (50), with $m = 0.2 = \mathrm{const}$. This value is very close to the LJ value

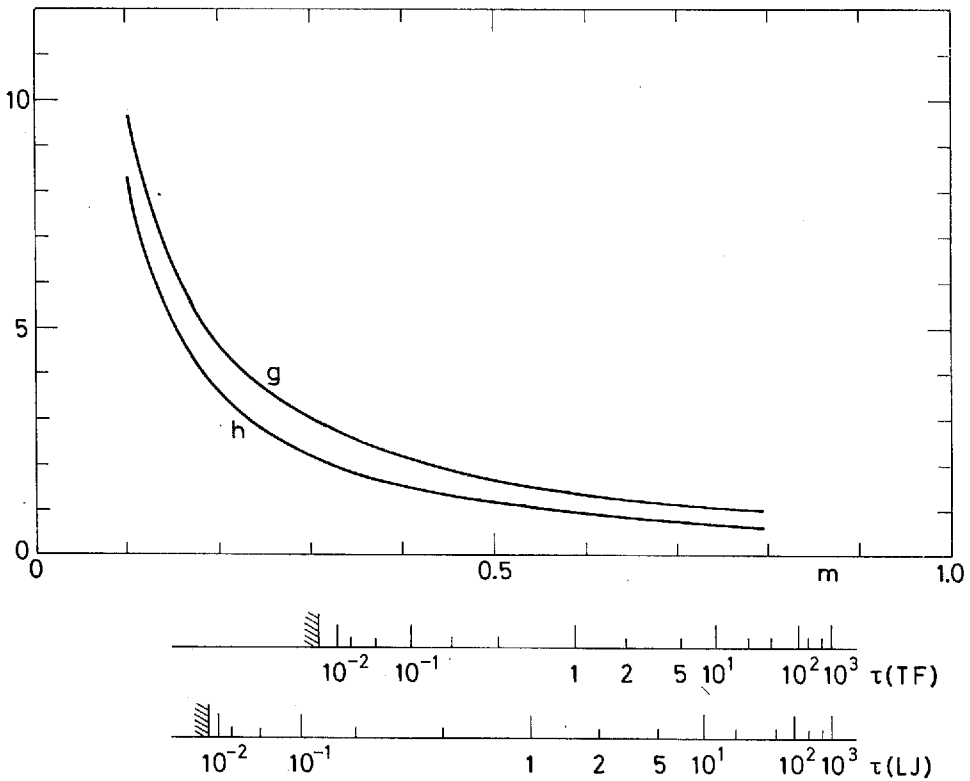

Fig. 5. The quantities g and h defined by eqs. (47a) and (51), respectively, versus power m. Scales of τ (48a) have been included by means of the relations derived in ref. 8.

0.191; it was chosen as the one extracted from measurements of the lateral half-width $\tilde{\varrho}_{1/2}$ on noble-gas targets[14] in the critical τ range $10^{-2} - 10^{-1}$. The TF curve has been included for comparison. Both the general trend, the region of the drop-off, and in particular the long-range limit are described quite well by the theoretical curve for $m = 0.2$. At the low τ values it is clearly superior to the TF-curve. Neither of them, however, explains the peculiar behaviour of the experimental points that is observed between $\tau = 1$ and 5.

10. Polyatomic Molecules

By application of the same physical model to a polyatomic molecule consisting of z atoms 1, 2, ... z, eqs. (7′) and (7) can be readily generalized,

$$\sigma(\mathbf{k}) = < \int d^2\mathbf{p}(1 - e^{i\mathbf{k}\cdot\sum_{i=1}^{z}\varphi_i(\mathbf{p}_i)}) \qquad (52')$$

and

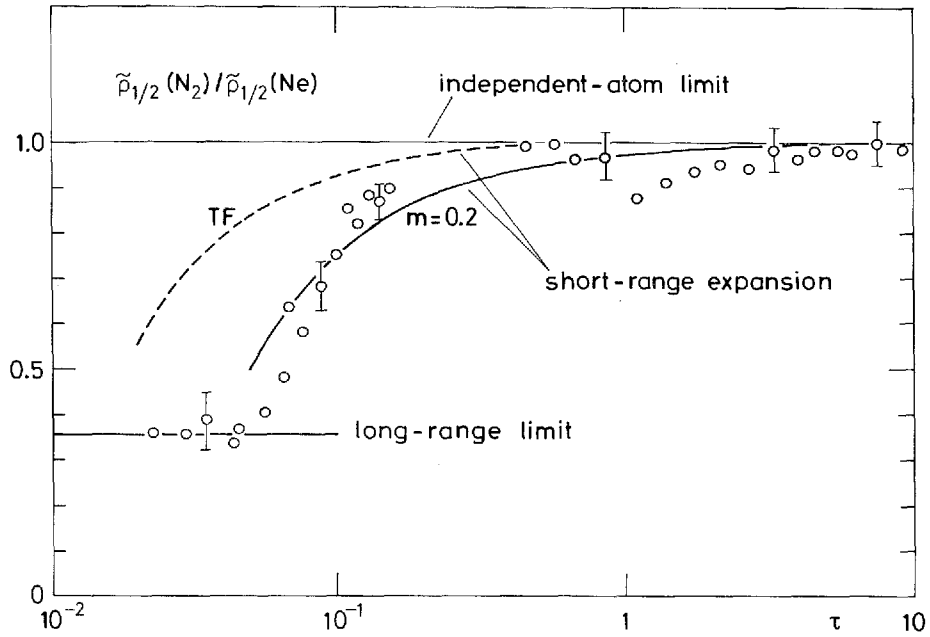

Fig. 6. Experimental ratio of lateral half-widths, $\tilde{\varrho}_{1/2}$ (nitrogen)$/\tilde{\varrho}_{1/2}$ (neon), versus thickness parameter τ (48a) from ref. 2. Fulldrawn curves: Eq. (50) for power $m = 0.2$ (Lenz-Jensen) at all τ. Dashed curve: Eq. (50) for Thomas-Fermi interaction.

$$\left.\begin{aligned}\sigma(\mathbf{k}) = \sum_i \sigma_i(k) - \sum_{i<j} \delta\sigma_{ij}(\mathbf{k}) + \sum_{i<j<k} \delta\sigma_{ijl}(\mathbf{k}) \ldots \\ \ldots + (-)^{z+1} \delta\sigma_{12\ldots z}(\mathbf{k})\end{aligned}\right\} \quad (52)$$

with $\sigma_i(\mathbf{k})$ defined by eq. (8) for $i = 1, 2, \ldots z$, and

$$\delta\sigma_{ij\ldots}(\mathbf{k}) = \langle \int d^2\mathbf{p}(1 - e^{i\mathbf{k}\cdot\varphi_i(\mathbf{p}_i)})(1 - e^{i\mathbf{k}\cdot\varphi_j(\mathbf{p}_j)}) \ldots \rangle; \quad (53a)$$

$\mathbf{p}_i$ is the (vectorial) impact parameter with atom i. The long-range limit is readily found from eq. (52′). Indeed, the leading term for small interatomic distances reads

$$\sigma(\mathbf{k}) \sim \int d^2\mathbf{p}(1 - e^{i\mathbf{k}\cdot\Sigma\varphi_i(\mathbf{p})}) \quad (53)$$

or, for power scattering, by means of (16) and (17),

$$\sigma(\mathbf{k}) \sim \left(\sum_1^z A_i^{\frac{1}{2m}}\right)^{2m} k^{2m}, \quad (54)$$

of which (18a) is a special case. In the short-range limit, eq. (52) yields

$$\sigma(\mathbf{k}) \sim \sum_i \sigma_i(\mathbf{k}) - \sum_{i<j} \frac{\sigma_i(k)\sigma_j(k)}{2\pi d_{ij}^2} + \sum_{i<j<k} \delta\sigma_{ijk}(k) \ldots \quad (55)$$

where d_{ij} is the distance between atoms i and j. The term $\delta\sigma_{ij}(\mathbf{k})$, according to its definition (53a), is equivalent with (9) for $i = 1$, $j = 2$, and is, therefore, identical with (13) for $1 = i$, $2 = j$. It will now be shown that except for a very small number of special cases, the subsequent terms in (55), from $\delta\sigma_{ijk}$ on, are of higher than second order in the inverse interatomic distance, and therefore have to be dropped.

Take the term $\delta\sigma_{123}$ as given by

$$\left.\begin{aligned}\delta\sigma_{123} &= \langle \int d^2\mathbf{p}(1 - e^{i\mathbf{k}\cdot\varphi_1(\mathbf{p}_1)})(1 - e^{i\mathbf{k}\cdot\varphi_2(\mathbf{p}_2)})(1 - e^{i\mathbf{k}\cdot\varphi_3(\mathbf{p}_3)})\rangle_\Omega \\ &= \prod_{i=1}\{\int d^2\mathbf{p}_i(1 - e^{i\mathbf{k}\cdot\varphi_i(\mathbf{p}_i)})\}\cdot\langle\delta(\mathbf{p}_1 - \mathbf{p}_2 - \mathbf{b}_{12})\delta(\mathbf{p}_1 - \mathbf{p}_3 - \mathbf{b}_{13})\rangle_\Omega\ ,\end{aligned}\right\} \tag{56}$$

where $\mathbf{b}_{ij}$ is the projection of the interatomic distance vector $\mathbf{d}_{ij}$ on the impact plane. Since only the leading term for large interatomic distances is of interest, we can simplify the rotational average

$$\langle\delta(\mathbf{p}_1 - \mathbf{p}_2 - \mathbf{b}_{12})\delta(\mathbf{p}_1 - \mathbf{p}_3 - \mathbf{b}_{13})\rangle_\Omega \sim \delta\langle(\mathbf{b}_{12})\delta(\mathbf{b}_{13})\rangle_\Omega\ . \tag{57'}$$

The operation $\langle\ldots\rangle_\Omega$ includes an integration over all orientations of an arbitrary rotational axis (here taken to be $\mathbf{d}_{12}$) and over the azimuthal angle of an arbitrary point within the molecule (here taken to be atom 3) with respect to that axis.

The azimuthal average is evaluated first. The factor $\delta(\mathbf{b}_{12})$ is not affected by this operation, but it ensures (by $b_{12} = 0$) that the rotational axis is identical with the polar axis of the system. Therefore,

$$\langle\delta(\mathbf{b}_{12})\delta(\mathbf{b}_{13})\rangle_\Omega = \langle\delta(\mathbf{b}_{12})\cdot\frac{\delta(b_{13})}{\pi b_{13}}\rangle = \frac{\delta(d_{13}\sin\varphi_{23})}{\pi d_{13}\sin\varphi_{23}}\langle\delta(\mathbf{b}_{12})\rangle.$$

Here, φ_{23} is the angle between $\mathbf{d}_{13}$ and $\mathbf{d}_{12}$, i.e. a fixed angle within the molecule, so that $b_{13} = d_{13}\sin\varphi_{23}$.

The average over the rotational axis reduces then to

$$\langle\delta(\mathbf{b}_{12})\rangle = \frac{1}{2\pi d_{12}^2}$$

a result which is identical with (12) for $\mathbf{p}_1 - \mathbf{p}_2 = 0$. Therefore,

$$\langle\delta(\mathbf{b}_{12})\cdot\delta(\mathbf{b}_{13})\rangle_\Omega = \frac{\delta(\sin\varphi_{23})}{2\pi^2 d_{12}^2 d_{13}^2\sin\varphi_{23}}, \tag{57}$$

and, from (56)

$$\delta\sigma_{123} \sim \frac{\sigma_1(k)\sigma_2(k)\sigma_3(k)}{2\pi^2 d_{12}^2 d_{13}^2}\cdot\frac{\delta(\sin\varphi_{23})}{\sin\varphi_{23}}. \tag{58}$$

Thus, for $\sin\varphi_{23} \neq 0$, we have $\delta\sigma_{123} = 0$ to order $d_{12}^{-2}\, d_{13}^{-2}$.

For a *linear* molecule, $\varphi_{23} = 0$, (58) becomes strongly divergent. In a real molecule, this divergence will be smeared out by molecular vibrations. Let, for example, φ_{23} be distributed according to a gaussian distribution

$$g(\varphi_{23})d^2\varphi_{23} = \frac{1}{2\pi\varphi_0{}^2}\, e^{-\frac{\varphi_{23}^2}{2\varphi_0{}^2}}\, 2\pi\varphi_{23}d\varphi_{23} \tag{59}$$

with a width $\varphi_0 \ll 1$, then $\langle \delta(\sin\varphi_{23})/\sin\varphi_{23}\rangle_g = \frac{1}{2\varphi_0{}^2}$, and

$$\langle \delta\sigma_{123}\rangle_g \sim \frac{\sigma_1\sigma_2\sigma_3}{(2\pi)^2 d_{12}{}^2 d_{13}{}^2 \varphi_0{}^2}. \tag{60}$$

This expression is negligible in comparison with, e.g., $\delta\sigma_{12}$, if

$$2\pi d_{13}{}^2\varphi_0{}^2 \gg \sigma_3 \tag{61}$$

The factor $\varphi_0{}^2$ makes this a rather strong requirement that will often not be fulfilled in cases of practical interest.

Therefore, the linear molecule needs to be treated separately, once more, and starting from (56). In such a molecule, we have, e.g.,

$$\mathbf{d}_{13} = \lambda \mathbf{d}_{12} \quad \text{with } \lambda \neq 0, \pm 1 \tag{62}$$

and hence

$$\mathbf{b}_{13} = \lambda \mathbf{b}_{12} \tag{62a}$$

Thus, the rotational average in (56) can be written

$$\left.\begin{aligned} \langle \delta(\mathbf{p}_1 - \mathbf{p}_2 - \mathbf{b}_{12})\delta(\mathbf{p}_1 - \mathbf{p}_3 - \mathbf{b}_{13})\rangle_\Omega &= \delta(\mathbf{p}_1 - \mathbf{p}_3 - \lambda(\mathbf{p}_1 - \mathbf{p}_2)) \cdot \\ \cdot \langle \delta(\mathbf{p}_1 - \mathbf{p}_2 - \mathbf{b}_{12})\rangle_\Omega &\sim \delta(\mathbf{p}_1 - \mathbf{p}_3 - \lambda(\mathbf{p}_1 - \mathbf{p}_2)) \cdot \frac{1}{2\pi d_{12}{}^2}. \end{aligned}\right\} \tag{63}$$

If this is inserted into (56), it becomes obvious that $\delta\sigma_{123} \propto d_{12}{}^{-2}$, i.e. of the same order as the $\delta\sigma_{ij}$ and therefore not negligible in general, for a linear molecule. The resulting expression

$$\left.\begin{aligned} \delta\sigma_{123} \sim \frac{1}{2\pi d_{12}{}^2} \int d^2\mathbf{p}_1 (1 - e^{i\mathbf{k}\cdot\varphi_1(\mathbf{p}_1)}) \int d^2\mathbf{p}_2 (1 - e^{i\mathbf{k}\cdot\varphi_2(\mathbf{p}_2)}) \cdot \\ \cdot (1 - e^{i\mathbf{k}\cdot\varphi_3(\mathbf{p}_1\cdot(1-\lambda)+\mathbf{p}_2\cdot\lambda)}) \end{aligned}\right\} \tag{64}$$

is a 2-center integral that can be evaluated by means of an expansion in Bessel functions, if needed. At present, we consider two limiting cases by means of a simple estimate.

We first note that the integrand in the expression

$$\sigma_i(k) = \int d^2\mathbf{p}(1 - e^{i\mathbf{k}\cdot\varphi_i(\mathbf{p})})$$

can be represented as a step function,

$$\left.\begin{aligned} 1 - e^{i\mathbf{k}\cdot\varphi_i(\mathbf{p})} \approx \begin{cases} 1 \ldots\ldots\ldots p \lesssim p_{0i}(k) \\ 0 \ldots\ldots\ldots p \gtrsim p_{0i}(k) \end{cases} \end{aligned}\right\} \tag{65}$$

since for small p, φ_i is large, and the exponential rapidly oscillating. By comparison with (17) and (17a) we find

$$p_{0i}(k) = \gamma_m (kC_i)^m \tag{65a}$$

with a well defined constant γ_m.

The following considerations refer, more or less explicitly, to a triatomic molecule. Take first the case where $p_{03}(k)$ is greater than $p_{01}(k)$ and $p_{02}(k)$, i.e., $C_3 > C_1, C_2$. Then, the integration region in (64) is determined essentially by p_{01} and p_{02}, and the last factor is 1 in that region. Then,

$$\delta\sigma_{123} \sim \frac{1}{2\pi {d_{12}}^2}\,\sigma_1\sigma_2 \sim \delta\sigma_{12};\ C_1, C_2 < C_3. \tag{66a}$$

In the opposite case, where p_{03} is substantially smaller than p_{01} and p_{02}, a similar consideration yields

$$\delta\sigma_{123} \ll \frac{\sigma_1\sigma_2}{2\pi {d_{12}}^2};\qquad C_1, C_2 \gg C_3. \tag{66b}$$

Now, C_i increases with increasing atomic number of the target atom. Therefore, the two limiting cases refer to molecules where one heavy atom (3) is surrounded by two light ones, and one light atom (3) surrounded by two heavy ones, respectively. For a triatomic molecule (55) yields

$$\sigma \sim \sigma_1 + \sigma_2 + \sigma_3 - \frac{\sigma_1\sigma_3}{2\pi {d_{13}}^2} - \frac{\sigma_2\sigma_3}{2\pi {d_{23}}^2} \quad \text{(atom 3 heavy)} \tag{67a}$$

and

$$\sigma \sim \sigma_1 + \sigma_2 + \sigma_3 - \frac{\sigma_1\sigma_2}{2\pi {d_{12}}^2} - \frac{\sigma_1\sigma_3}{2\pi {d_{13}}^2} - \frac{\sigma_2\sigma_3}{2\pi {d_{23}}^2} \quad \text{(atom 3 light)} \tag{67b}$$

The latter result does not differ from what would be expected for a nonlinear triatomic molecule. And the former result (67a) could just as well have been derived by means of the fact that the term $\delta\sigma_{12} \sim \frac{\sigma_1\sigma_2}{2\pi {d_{12}}^2}$ would be smaller than $\delta\sigma_{13}$ and $\delta\sigma_{23}$, both because $\sigma_1, \sigma_2 \ll \sigma_3$ and $d_{12} > d_{13}, d_{23}$. It thus appears that the only case where some uncertainty prevails is that of a linear molecule with 3 roughly equal constituents. In that case, we have

$$\frac{\sigma_1\sigma_3}{2\pi {d_{13}}^2} \approx \frac{\sigma_2\sigma_3}{2\pi {d_{23}}^2} \approx 4\,\frac{\sigma_1\sigma_2}{2\pi {d_{12}}^2} \tag{68}$$

if 1 and 2 are the outer atoms. Thus, the uncertainty due to lack of knowledge of the accurate value of the sum $-\delta\sigma_{12} + \delta\sigma_{123}$ is $\sim$ 12 pct. of $\delta\sigma_{13} + \delta\sigma_{23}$, i.e. a 12 pct. error in a correction. This must most often be an acceptable uncertainty.

It, occurs therefore, that at least for triatomic molecules, the expression

$$\sigma(k) \sim \sum_{i=1}^{z} \sigma_i(k) - \sum_{i<j} \frac{\sigma_i(k)\,\sigma_j(k)}{2\pi d_{ij}^2} \tag{69}$$

gives a satisfactory estimate of the transport cross section in the short-range limit, independent of the detailed geometry of the molecule.

In atoms containing more than three molecules, similar considerations would have to be applied to terms of the type $\delta\sigma_{1234}$ etc. The type of argument would be the same as what was applied in this section, and the results would be similar. A case where caution would have to be applied is that of long chain molecules ("strings"). Other types of processes[16] that are outside the scope of this paper would have to be considered there.

11. Polyatomic Molecules: Single Scattering

Single-scattering cross sections for polyatomic molecules are established readily be means of eqs. (54) and (69) from eq. (4). The results are straight generalizations of those quoted in sect. 6 for diatomic molecules. They read

$$\frac{d\sigma}{d\varphi} = \sum_i \frac{d\sigma_i}{d\varphi} - \frac{R(m)}{m} \sum_{i<j} \frac{\varphi}{2\pi d_{ij}^2} \frac{d\sigma_i}{d\varphi} \cdot \frac{d\sigma_j}{d\varphi} \cdots \tag{70a}$$

for small interaction distance, and

$$\frac{d\sigma}{d\varphi} = \left(\sum_i \left(\frac{d\sigma_i}{d\varphi} \right)^{\frac{1}{2m}} \right)^{2m} \cdots \tag{70b}$$

in the long-range limit. $R(m)$ is defied by eq. (21) and plotted in fig. 3. Both equations show that the relative magnitude of molecular corrections in comparison with the independent-atom limit ($d_{ij} = \infty$) increases with increasing number of atoms per molecule. The conclusions made in sect. 6 remain otherwise unchanged.

If the molecule is built up of z atoms with similar atomic numbers and masses, we can ignore the differences between the constituents, and write eqs. (70) in the form

$$\frac{d\sigma}{d\varphi} \simeq z \frac{d\sigma_1}{d\varphi} - \frac{R(m)}{m} \varphi \left(\frac{d\sigma_1}{d\varphi} \right)^2 \sum_{i<j} \frac{1}{2\pi d_{ij}^2} \cdots \tag{70a'}$$

$$\frac{d\sigma}{d\varphi} = z^{2m} \frac{d\sigma_1}{d\varphi} \cdots \tag{70b'}$$

Thus, the two limiting cases differ by a factor of z^{2m-1}; since the long-range limit applies mainly to collisions where $m \lesssim 0.2$ (LJ), this ratio decreases substantially with increasing z. When the sum in (70a') is written in the form

$$\sum_{i<j} \frac{1}{2\pi d_{ij}^2} = < \frac{1}{2\pi d_{ij}^2} > \tfrac{1}{2} z(z-1), \tag{71}$$

it becomes evident that the molecular correction to the independent-atom limit increases like $z-1$ on a relative scale for small molecules ($z \lesssim 5$), but more slowly for larger ones.

These relations can easily be written in terms of TF variables (28). However, TF variables provide a substantial simplification only for homonuclear (or approximately homonuclear) molecules.

12. Polyatomic Molecules: Multiple Scattering

The generalization to polyatomic molecules of the relations derived in sect. 8 for multiple scattering starts also with eqs. (54) and (69), and eqs. (35) and (36). Instead of (41) and (42), we obtain

$$\frac{(\alpha_{1/2})_{\text{mol}}}{(\alpha_{1/2})_{\text{dissoc}}} = \frac{(\varrho_{1/2})_{\text{mol}}}{(\varrho_{1/2})_{\text{dissoc}}} = \frac{\sum_i C_i}{(\sum_i C_i^{2m})^{1/2m}} \tag{72}$$

in the long-range limit. This approaches $z^{1-1/2m}$ for homonuclear molecules.

For nearly independent atoms, we obtain the following relations instead of (44′) and (46′),

$$\frac{(\alpha_{1/2})_{\text{mol}}}{(\alpha_{1/2})_{\text{dissoc}}} \cong 1 - \frac{g}{2m} \cdot \frac{1}{(\sum_i A_i)^2} \sum_{i<j} \frac{A_i A_j}{2\pi d_{ij}^2 N' x} \tag{73a}$$

$$\frac{(\varrho_{1/2})_{\text{mol}}}{(\varrho_{1/2})_{\text{dissoc}}} \cong 1 - \frac{g}{2m} \frac{(2m+1)^2}{4m+1} \frac{1}{(\sum_i A_i)^2} \sum_{i<j} \frac{A_i A_j}{2\pi d_{ij}^2 N' x} \tag{73b}$$

where A_i and g are given by (17a) and table I, respectively.

In case of (approximately) homonuclear target molecules, (73a) reads

$$\frac{(\alpha_{1/2})_{\text{mol}}}{(\alpha_{1/2})_{\text{dissoc}}} \cong 1 - \frac{g}{2m} \frac{1}{z^2} \sum_{i<j} \frac{1}{2\pi d_{ij}^2 N' x} = 1 - \frac{g}{2m} \cdot \frac{z-1}{2} < \frac{1}{2\pi d_{ij}^2 N x} > \tag{73a'}$$

where $N = zN'$ is the number of atoms per unit volume. Obviously, the molecular correction to the independent-atom limit increases with increasing z in much the same way as was found in case of the single-scattering cross section. The corresponding relations for $\varrho_{1/2}$, and the equations for TF-scaled quantities (in the homonuclear case) are easily found.

13. Summary

1. In the classical small-angle scattering of charged particles by molecules it is convenient to define three regions; a long-range limit, where the interaction takes place at a sufficiently large distance so that the molecule acts as one target particle; a short-range limit where the interaction takes place at sufficiently small distances so that each constituent atom (if close enough to the orbit) acts as one target particle; and a transition region.

2. In single scattering, the long-range limit is reached at low energies and/or small scattering angles. The reverse is true for the short-range limit. The transition region covers the range $10^{-2} \lesssim \eta (= t^{1/2}) \lesssim 1$ in Thomas Fermi variables. This corresponds to moderate screening of the Coulomb interaction. Typical measurements of incomplete total cross sections trace the region of excessive screening ($\eta \ll 10^{-2}$); the long-range limit applies to those situations.

3. In multiple scattering, the long-range limit applies to small values of the thickness parameter $\tau = \tau a^2 N x$, and large ones for the short-range limit. The transition region covers the range $10^{-2} \lesssim \tau \lesssim 1$.

4. The short-range limit can be realized experimentally by means of a dissociated gas target, or a noble-gas target with similar atomic number. The single-collision cross section of the molecular gas (differential or total) is smaller by up to a factor of the order of $\sim z^{2m-1} \approx z^{-0.6}$ than the corresponding quantity for the dissociated gas, where z is the number of atoms in the molecule. Multiple-scattering half-widths (angular or lateral) are smaller by up to a factor of $\sim z^{1-1/2m} \approx z^{-3/2}$.

5. The calculations presented here are based on the simplifying assumption of a target molecule composed of undisturbed, spherically symmetric atoms that are arranged in some geometric configuration; i.e., valence effects are ignored. Since the transition region between the long- and short-range limit lies entirely in the Thomas-Fermi region of the scattering diagram where valence effects are unimportant, this simplifying assumption only affects the detailed behaviour *within* the long-range limit. The quantitative results presented in this paper refer to the deviations from an independent-atom picture, i.e. the short-range limit and the transition region; these results are insensitive to valence effects.

6. For essentially the same reason, the exclusive use of a classical-orbit picture of the scattering process is not a severe limitation.

7. Experimental data on single scattering off molecules in the transition region do not appear to be available. One recently published set of multiple-scattering half-widths on nitrogen is in excellent agreement with the theoretical prediction, both in the long-range limit and the transition region, provided that the scattering law for individual atoms is chosen in accordance with the experimentally found multiple-scattering half-widths on noble gases. This scattering law corresponds much closer to Lenz-Jensen than to Thomas-Fermi screening. The multiple-scattering half-width in the transition region is quite sensitive to the scattering law for individual atoms. Therefore, the molecular effect described in this paper serves as an additional probe for interatomic potentials in the moderately-screened Coulomb region.

8. With respect to practical applications in accelerator physics, it may be useful to recall that regardless of the nature of the target molecule, target pressure, and ion type and energy, the multiple-scattering distribution is narrower for the molecular than for the dissociated gas, so long as the small-angle approximation applies.

Acknowledgements

This work was stimulated by Georg Sidenius' insistence that a molecule is not just the sum of its atoms. A major incitament was the close cooperation with the experimental groups in Copenhagen, N. Andersen and G. Sidenius, and in Aarhus, F. Besenbacher, J. Heinemeier, P. Hvelplund, and H. Knudsen. Special thanks are due to J. Schou for checking some of the integrals, and to N. Andersen for numerous discussions. A. Russek made valuable comments on the manuscript.

Appendix A

This appendix serves to specify the median values k_0 and $\varkappa_0$ as representative values of k and $\varkappa$ in Bothe's formula (35) and its modification (36) for lateral profiles. Consider (35) first and define k_0 by the relation

$$\frac{1}{2\pi}\int_0^{k_0} dk\, k J_0(k\alpha)\, e^{-N' x \sigma(k)} = \frac{1}{2\pi}\int_{k_0}^{\infty} dk\, k J_0(k\alpha)\, e^{-N' x \sigma(k)}, \qquad \text{(A1)}$$

i.e., k_0 divides up the integration into two equal parts. For values of α within the half-width $\alpha_{1/2}$, one may set $\alpha = 0$ without making a serious error. Then, k_0 becomes independent of α, and (A1) has a unique solution.

(A1) is rewritten by means of (18).

$$\int_0^{k_0} dk\, k e^{-N'xAk^{2m}} = \tfrac{1}{2}\int_0^{\infty} dk\, k e^{-N'xAk^{2m}} \tag{A2}$$

or, after introduction of the variable

$$t = N'xAk^{2m}, \tag{A3}$$

$$\int_0^{g} dt\, t^{\frac{1}{m}-1} e^{-t} = \tfrac{1}{2}\int_0^{\infty} dt\, t^{\frac{1}{m}-1} e^{-t}, \tag{A4}$$

where

$$g = N'xAk_0^{2m}; \tag{A5}$$

In terms of an incomplete gamma function[17], (A4) reads

$$P\left(\frac{1}{m}, g\right) = \tfrac{1}{2}; \tag{A6}$$

This determines $g = g(m)$. Table I shows g as evaluated from the tables in ref. 17. Insertion of (A5) into (44) with $A = A_1 + A_2$ yields (44′) and (47).

By applying the same argument to the lateral distribution (36), the equation that corresponds to (A2) reads

$$\int_0^{\varkappa_0} d\varkappa\, \varkappa e^{-N'\frac{x^{2m+1}}{2m+1}A\varkappa^{2m}} = \tfrac{1}{2}\int_0^{\infty} d\varkappa\, \varkappa e^{-N'\frac{x^{2m+1}}{2m+1}A\varkappa^{2m}}. \tag{A7}$$

The proper variable is now

$$t = N'\frac{x^{2m+1}}{2m+1}A\varkappa^{2m} \tag{A8}$$

and

$$g = N'\frac{x^{2m+1}}{2m+1}a\varkappa_0^{2m} \tag{A9}$$

with g being a solution of (A6). (A9) inserted into (46) yields (46′) and (47).

Appendix B

It is the purpose of this appendix to provide a somewhat more quantative argument for the claim that a molecular multiple-scattering profile approaches the independent-atom profile at larger scattering angles. Only the angular profile $F(x,\alpha)$ will be considered. The procedure is a generalization of the perturbation approach taken in sect. 8.

Take eq. (35) and insert (14),

$$F(x,\alpha) \cong \frac{1}{2\pi}\int_0^\infty k dk J_0(k\alpha) e^{-N'x\left(\sigma_1(k)+\sigma_2(k)-\frac{\sigma_1(k)\sigma_2(k)}{2\pi\bar{a}^2}\right)} \tag{B1}$$

for x sufficiently large so that the molecular correction is small. Within the perturbation approach, we can write

$$F(x,\alpha) \approx e^{N'x\frac{\sigma_1(k_1)\sigma_2(k_1)}{2\pi\bar{a}^2}} \cdot \frac{1}{2\pi}\int_0^\infty k dk J_0(k\alpha) e^{-N'x(\sigma_1(k)+\sigma_2(k))}, \tag{B2}$$

where

$$k_1 = k_1(\alpha) \tag{B3}$$

is the median value of the integral (B2). Therefore, (B2) can be written in the form

$$F(x,\alpha) \cong S(\alpha) \cdot F_{at}(x,\alpha) \tag{B4}$$

where $F_{at}(x,\alpha)$ is the independent-atom distribution, and

$$S(\alpha) = e^{N'x\frac{\sigma_1(k_1)\sigma_2(k_1)}{2\pi\bar{a}^2}} \tag{B5}$$

This function is greater than 1 for $\alpha = 0$, and decreases towards 1 with increasing α, since $k_1(\alpha)$ decreases. An approximate expression for $k_1(\alpha)$ is found by series expansion,

$$J_0(k\alpha) \approx 1 - k^2\alpha^2/4; \tag{B6}$$

$$k_1(\alpha) \approx k_0 - r_0\alpha^2 \tag{B7}$$

where k_0 is defined by eq. (A2). The requirement of $k_1(\alpha)$ being a median value yields, then, to first order in α^2, the following expression for r_0,

$$\left.\begin{aligned} r_0 = \frac{e^{N'x[\sigma_1(k_0)+\sigma_2(k_0)]}}{8k_0}\Bigg\{\int_0^\infty dk\, k^3 e^{-N'x(\sigma_1(k)+\sigma_2(k))} \\ - 2\int_0^{k_0} dk\, k^3 e^{-N'x(\sigma_1(k)+\sigma_2(k))}\Bigg\}; \end{aligned}\right\} \tag{B8}$$

In the notation of appendix A, this can be written

$$r_0 = \Gamma(2/m)(1 - 2P(2/m,g))\frac{e^g}{16m} \cdot k_0^{-1} \cdot (N'xA)^{-2/m}. \tag{B9}$$

From this, and (B7), we obtain

$$S(\alpha) \cong 1 + \frac{g^2 A_1 A_2}{2\pi d^2 N' x (A_1 + A_2)^2} \left[1 - B(m) \left(\frac{\alpha}{2[gN'x(A_1 + A_2)]^{1/2m}} \right)^2 \right] \qquad \text{(B10)}$$

where

$$B(m) = \Gamma(2/m)\,(1 - 2P(2/m,g))e^g \qquad \text{(B11)}$$

(B10) shows that the zero-angle scattering intensity is greater than its independent-atom value by an amount that corresponds to the decrease in half-width (44′) due to the molecular correction. With increasing angle, this enhancement approaches zero.

References

1. P. Sigmund, Phys. Rev. A. **14**, 996 (1976).
2. G. Sidenius, N. Andersen, P. Sigmund, F. Besenbacher, J. Heinemeier, P. Hvelplund, and H. Knudsen, Nucl. Inst. Meth. **134**, 597 (1976).
3. N. Bohr, Mat. Fys. Medd. Dan. Vid. Selsk. **18**, no. 8 (1948).
4. J. Lindhard, V. Nielsen, and M. Scharff, ibid. **36**, no. 10 (1968).
5. U. Buck, Rev. Mod. Phys. **46**, 369 (1974).
6. P. Sigmund, *in* Physics of Ionized Gases, M. Kurepa, editor, Institute of Physics, Belgrade, p. 137 (1972).
7. P. Sigmund and K. B. Winterbon, Nucl. Inst. Meth. **119**, 541 (1974); ibid. **125**, 491 (1975).
8. A. D. Marwick and P. Sigmund, Nucl. Inst. Meth. **126**, 317 (1975).
9. K. B. Winterbon, P. Sigmund, and J. B. Sanders, Mat. Fys. Medd. Dan. Vid. Selsk. **37**, no. 14 (1970).
10. H. van Dop, A. J. H. Boerboom, and J. Los, Physica **61**, 626 (1972).
11. P. Loftager and G. Claussen, Proc. Int. Conf. Electronic and Atomic Collisions, Boston, Mass. (1969), p. 518.
12. K. B. Winterbon, Rad. Effects **13**, 215 (1972).
13. G. Sidenius and N. Andersen, Nucl. Inst. Meth. **128**, 271 (1975); ibid. **131**, 387 (1975).
14. F. Besenbacher, J. Heinemeier, P. Hvelplund, and H. Knudsen, Phys. Rev. A. **13**, 2095 (1976).
15. B. Efken, D. Hahn, D. Hilscher, and G. Wüstefeld, Nucl. Instr. Meth. **129**, 227 (1975)
16. J. Lindhard, Mat. Fys. Medd. Dan. Vid. Selsk. **34**, no. 14 (1965).
17. M. Abramowitz and I. Stegun, Handbook of Mathematical Functions, Dover Publ. Inc., New York (1964).
18. R. J. Glauber, Phys. Rev. **100**, 242 (1955).

Peter Sigmund
Physical Laboratory II
H. C. Ørsted Institute
DK–2100 Copenhagen Ø.

Indleveret til Selskabet oktober 1976.
Færdig fra trykkeriet juni 1977.